

Measuring Integrin Force Loading Rates Using a Two-Step DNA Tension Sensor

J. Dale Combs,[§] Alexander K. Foote,[§] Hiroaki Ogasawara, Arventh Velusamy, Sk Aysha Rashid, Joseph Nicholas Mancuso, and Khalid Salaita*



Cite This: *J. Am. Chem. Soc.* 2024, 146, 23034–23043



Read Online

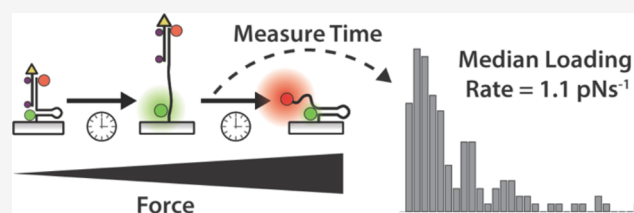
ACCESS |

Metrics & More

Article Recommendations

Supporting Information

ABSTRACT: Cells apply forces to extracellular matrix (ECM) ligands through transmembrane integrin receptors: an interaction which is intimately involved in cell motility, wound healing, cancer invasion and metastasis. These small (piconewton) integrin-ECM forces have been studied by molecular tension fluorescence microscopy (MTFM), which utilizes a force-induced conformational change of a probe to detect mechanical events. MTFM has revealed the force magnitude for integrin receptors in a variety of cell models including primary cells. However, force dynamics and specifically the force loading rate (LR) have important implications in receptor signaling and adhesion formation and remain poorly characterized. Here, we develop an LR probe composed of an engineered DNA structure that undergoes two mechanical transitions at distinct force thresholds: a low force threshold at 4.7 pN (hairpin unfolding) and a high force threshold at 47 pN (duplex shearing). These transitions yield distinct fluorescence signatures observed through single-molecule fluorescence microscopy in live cells. Automated analysis of tens of thousands of events from eight cells showed that the bond lifetime of integrins that engage their ligands and transmit a force >4.7 pN decays exponentially with a τ of 45.6 s. A subset of these events mature in magnitude to >47 pN with a median loading rate of 1.1 pN s⁻¹ and primarily localize at the periphery of the cell–substrate junction. The LR probe design is modular and can be adapted to measure force ramp rates for a broad range of mechanoreceptors and cell models, thus aiding in the study of molecular mechanotransduction in living systems.



INTRODUCTION

Many important biomolecular interactions involved in sustaining life are regulated through small, piconewton (pN) scale forces. These forces, applied to and by the cells through membrane receptors such as integrins, play a pivotal role in transducing signals into downstream biochemical pathways, a process described as mechanotransduction.^{1–4} The process of interconverting mechanical cues into biochemical signals is critical to a vast array of biological processes, including wound healing, cell motility, and tissue fibrosis.^{5–8} Molecular tension fluorescence microscopy (MTFM) probes have been developed to measure and analyze the pN forces transmitted at cell–extracellular matrix (ECM) and cell–cell interfaces, employing extendable molecules such as polyethylene glycol (PEG),^{9,10} DNA,¹¹ and proteins¹² that are flanked by fluorescent donor–acceptor pairs.^{13–16} Studies employing molecular tension probes have demonstrated that integrins sense and activate mechanotransduction pathways in response to pN forces.^{17–21} While existing probes have revealed the magnitude of forces transmitted by integrins, the force dynamics remain unclear, particularly at the single-molecule scale. Quantifying integrin force dynamics is critical, as dynamics are important parameters in studying adhesions²² and understanding how various integrin-targeting drugs modulate function.^{3,23–26}

Indeed, there has been much speculation about the integrin force loading rate (LR), which has been estimated from bulk measurements of the deformation of elastomeric substrates with values ranging from 0.007 pN s⁻¹ up to 4 pN s⁻¹.²⁷

One potential approach to measuring the LR is to perform time-dependent single-molecule measurements of the MTFM probes. However, this is a challenge because it is difficult to characterize single-molecule fluorescence dynamics for weak and transient signals that are prone to photobleaching in the presence of living cells that generate autofluorescence. To address these problems, we created a force LR probe with two enabling features. First, the probe undergoes two digital mechanical transitions at distinct forces identified by unique fluorescence signatures (Figure 1a).^{11,28} This strategy avoids the ambiguity of analog sensors.^{29–31} Second, we engineered the LR probe with dual quenchers that significantly suppress photobleaching.

Received: March 14, 2024

Revised: July 22, 2024

Accepted: July 24, 2024

Published: August 12, 2024



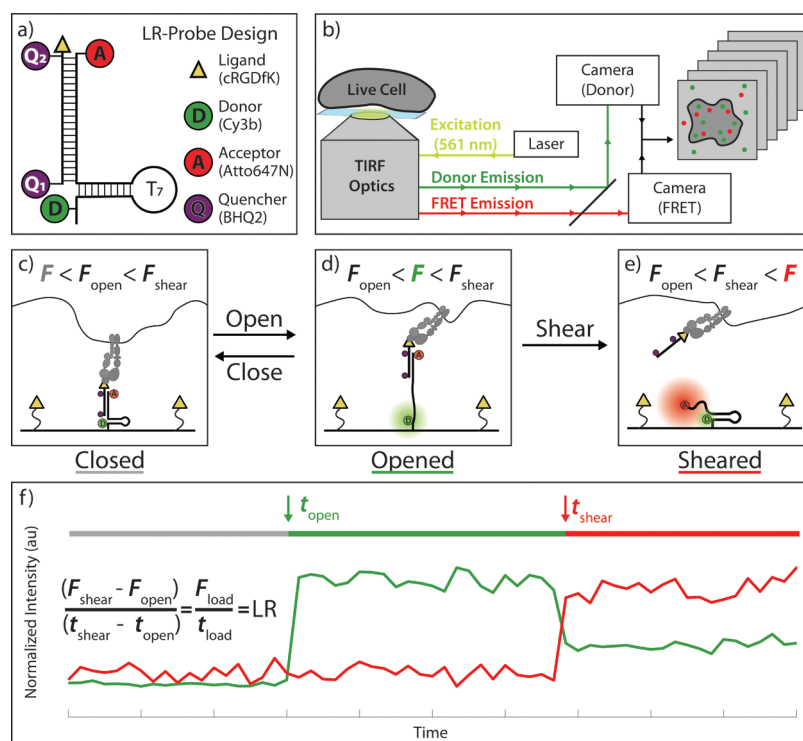


Figure 1. Schematic of LR probe and expected data. (a) LR probe schematic. (b) Optical diagram showing microscope setup used for single-molecule fluorescence microscopy of LR probe. (c) Schematic showing initial integrin engagement with LR probe at low force ($F < 4.7$ pN) resulting in the probe in the closed state. Both donor and fluorescence resonance energy transfer (FRET) signals are quenched in the closed state. (d) $F > 4.7$ pN but < 47 pN place the probe in the opened state which is characterized by donor turn-on signal and lack of FRET signal. (e) Forces > 47 pN result in probe shearing characterized by FRET emission and diminished donor signal. (f) Idealized donor/FRET trajectory, showing times when the probe opened (t_{open}) and sheared (t_{shear}), and marking the opened and sheared states with a green and red line. Force values for opening and shearing and the timestamps of each transition are used to calculate the loading rate (LR).

The LR probe was composed of two oligonucleotide strands: a ligand strand and an anchor strand (SI Note 1, LR Probe Concept; SI Note 2, LR Probe Synthesis). The anchor folds into a hairpin and is modified with both a donor dye (Cy3B) and a FRET acceptor dye (Atto647N). The ligand strand presents a cyclic RGDfK (cRGD) peptide, contains two quenchers (Q_1 and Q_2), and is complementary to the anchor strand. The fluorescent output of the LR probe informs on its mechanical state and can be used to infer the force dynamics of the integrin-ligand bond. Time-dependent single-molecule imaging of the LR probe was performed by directly exciting the donor while simultaneously collecting fluorescence from both the donor and FRET channels (Figures 1b and S1). When the LR probe is in its closed state and little to no force is applied, both dyes are quenched, reducing fluorescent output to near-background (Figure 1c,f). The hairpin domain of the LR probe unfolds when $F > 4.7$ pN is applied, which is associated with early loading by integrin receptors (Figure 1d).¹¹ Note that the 4.7 pN value represents the $F_{1/2}$ which is the equilibrium unfolding force.²⁸ This unfolding transition leads to a separation of the donor and Q_1 , resulting in a distinct turn-on signal of donor emission (Figure 1d,f). As the tension on the probe increases, the ligand strand undergoes irreversible shearing at $F > 47$ pN which is the threshold for duplex shearing (Figure 1e).^{32,33} Note that the force required to cause this shearing event is dependent on the loading rate, and thus a loading-rate-dependent model was used to determine this F_{shear} value (see SI Note 3, Modeling of F_{shear} with variable loading rate).³⁴ Shearing leads to loss of the ligand strand containing both quenchers, allowing for probe refolding and a

corresponding turn-on of the FRET signal (Figure 1e,f). Figure 1f shows an idealized representation of fluorescence readout and marks the timestamps of these transitions (t_{open} and t_{shear}). By measuring the time between hairpin opening (t_{open} , marked by donor turn-on) and duplex shearing (t_{shear} , marked by FRET emission) using single-molecule fluorescence microscopy, we can estimate the loading rate between those two events in live cells within functional adhesions. Importantly, the loading rate is inferred from two discrete timestamps: when the LR probe opens at $F > F_{\text{open}}$, and when the LR probe is sheared at $F > F_{\text{shear}}$. As such, the measured loading rate is an average, or a linear approximation, of the time between these two force thresholds. We will refer to this average loading rate as simply the “loading rate” in this work. The actual loading dynamics are likely much more complex but difficult to detect with single-molecule resolution. A direct observation of LR requires time-dependent measurements of probe extension,³¹ which is noisy and necessitates ensemble averaging. Our methodology allows for discrete, clearly observable timestamps for each integrin, which, while easy to interpret, necessarily limits the observed rate to an average between those timestamps.

RESULTS

Characterizing the LR Probe. The experimental procedure for probe synthesis, surface preparation, and live-cell imaging are found in SI Notes 2, 4, and 5 and are labeled, respectively. To validate the LR probe as a single-molecule force sensor, we performed a series of controls to characterize

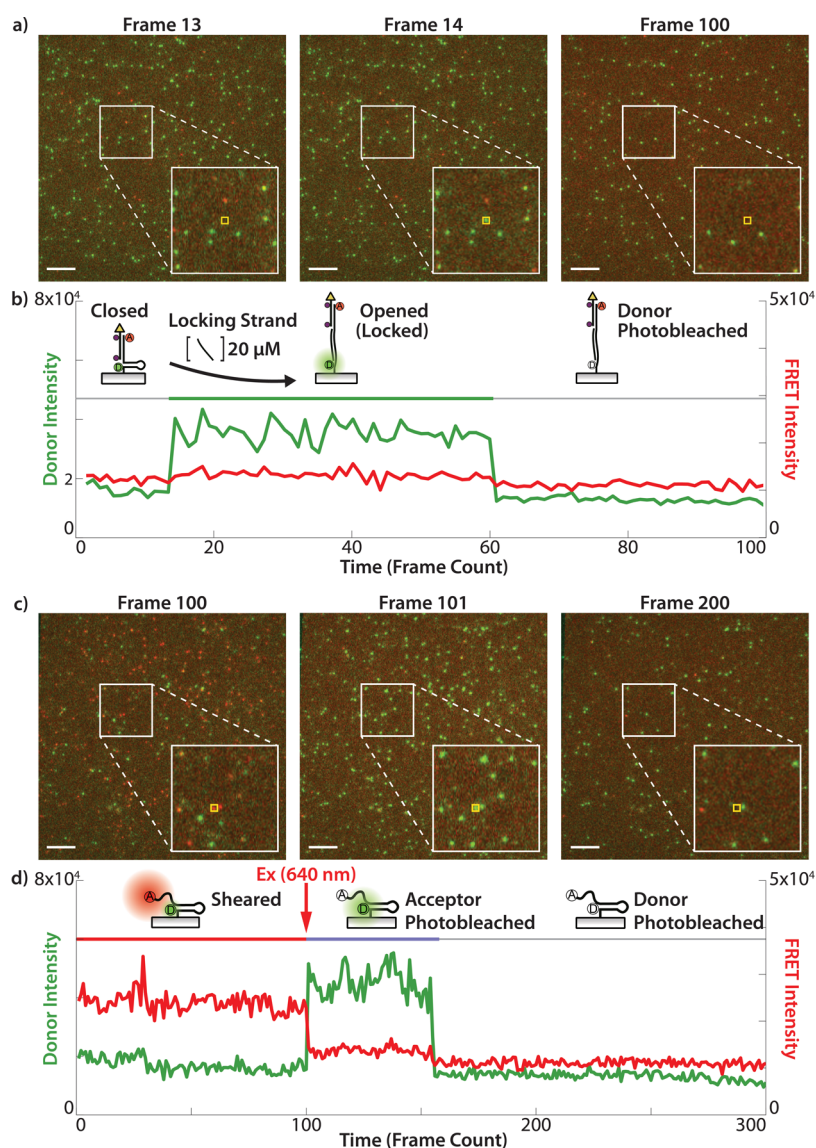


Figure 2. LR probe single-molecule fluorescence emission validation. (a) Representative images from a timelapse of a surface with LR probe showing donor (green) and FRET (red) fluorescent signal. The white inset shows a 100×100 pixel region, and the further yellow inset shows a 5×5 region highlighting a single molecule. Frame 13 shows the probe in the closed state, Frame 14 shows the probe is locked into the opened state with its complement strand, and Frame 100 shows the signal has photobleached. Scale bars = $10 \mu\text{m}$ for entire figure. (b) Time trace of the total fluorescent signal within the yellow 5×5 region marked in (a), with the probe's state assignment shown with the horizontal colored bar. (c) Representative images from a timelapse of a surface with a sheared LR probe which begins in a high-FRET state with insets matching those in (a). Frame 100 shows the probe in a high-FRET state; photobleaching is induced between Frame 100 and 101, and Frame 101 shows diminished FRET and recovered donor signal. By Frame 200, the donor has photobleached. (d) Time trace of the fluorescent signal from the experiment shown in (c).

the signal associated with its state transitions (closed, opened, and sheared, Figure 1c–e). The first control experiment characterized the signal associated with opening of the DNA hairpin with $F > 4.7$ pN (closed \rightarrow opened transition). This transition was mimicked by first measuring a closed LR probe on a surface and then adding (at frame 0) a 17-mer complement ($20 \mu\text{M}$) to the hairpin stem loop which irreversibly locks the DNA hairpin into the opened state. To anchor the LR probe to the glass surface, we grafted a dense layer of biotinylated-PEG onto the surface modified with streptavidin (SI Note 4, LR Probe Surface Preparation).³⁵ Note that previous work shows that biotinylated DNA primarily binds in a monomeric fashion when incubated at low concentrations with streptavidin surfaces.³⁶ We sub-

sequently added the LR probe (400 pM concentration) to achieve a sparse density of probes appropriate for single-molecule imaging (Figures 2a and S2, S3). Figure 2a shows representative fluorescent images from both the donor (green) and FRET (red) channels at time points that highlight the closed-to-opened state transition. These images show the entire field of view, with a white inset highlighting a 100×100 pixel region and a further yellow inset highlighting a 5×5 pixel region which marks the location of a single molecule. The donor and FRET signals within this 5×5 region were summed to show their intensity as a function of time (Figure 2b). From this trace, it is clear that the probe starts in the closed state (frames 0–13, low donor and FRET signal), transitions to an opened state (frames 14–60, high donor and low FRET

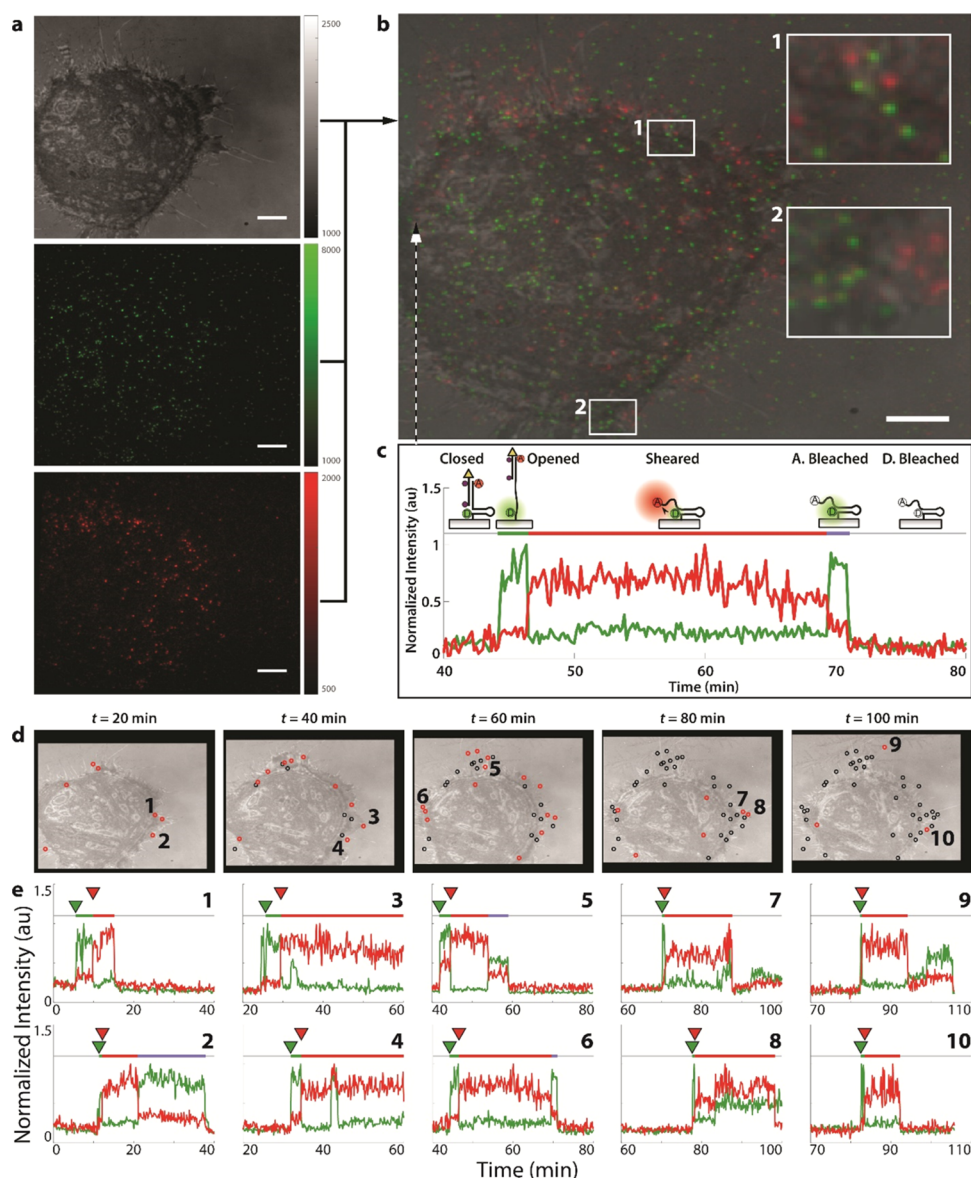


Figure 3. Single-molecule analysis of live-cell adhesions using LR probe. (a) RISM (top), donor (middle), and FRET (bottom) images at $t = 0$. Scale bar = $10 \mu\text{m}$, and the vertical intensity bars show raw electron-multiplying charge-coupled device (EMCCD) pixel intensity. (b) Overlay of images (a), with two highlighted regions showing single-molecule puncta observed. (c) Fluorescence time trace of the 3×3 pixel region shown with an arrow. This time trace exhibits the closed \rightarrow opened \rightarrow sheared transitions as seen in the donor (green) and FRET (red) intensities and marks the opened, sheared, and acceptor photobleached state of the probe with a green, red, and purple horizontal line, respectively. (d) Images of the cell at 20 min intervals, with red circles marking locations of shearing events occurring during that interval. Shearing events are carried over between frames as black circles, showing a buildup of events. Numbers 1–10 correspond to the fluorescent trajectories shown below. (e) Fluorescent trajectories matching the color schematic in (c), with green and red arrows showing the timestamps of the opening transition (t_{open}) and shearing transition (t_{shear}), respectively. Locations are marked in (d).

signal), and exhibits single-step photobleaching of the donor (frames 61 onward). Above the intensity trajectory in Figure 2b, we mark with a green line the opened state probe, which is followed by donor photobleaching. Further controls were performed quantifying the negligible bleed-through of the donor dye into the FRET channel (Figure S4), the rate of donor photobleaching (Figure S5), and the kinetics of the LR probe opening through its complement locking strand (Figure S6). The kinetics of hairpin locking are similar to those previously characterized in ensemble measurements.³⁷ Finally, additional traces from these images were analyzed to show that the signal consistently exhibited single-step photobleaching

(Figure S7). This shows that the fluorescent puncta observed in this experiment are primarily due to single molecules.

Having identified the signal produced by both the closed and opened states of the probe, we next characterized the signal produced by the sheared state, which occurs at $F > 47$ pN (opened \rightarrow sheared transition). Shearing of the ligand strand allows the DNA hairpin to refold without the dual quenchers. This process activates the FRET between Cy3B and Atto647N, turning on the FRET signal while diminishing the Cy3B emission. The sheared state of the LR probe was formed by attaching the probe to the surface without the top ligand strand (Figure 2d, probe drawing). Figure 2c shows representative images of the fluorescent readout, with white

and yellow insets marking the corresponding 100×100 and 5×5 pixel regions, as described previously. The fluorescence image at frame 100 shows many probes with the majority displaying high FRET, indicative of the sheared state. To induce photobleaching of the acceptor, we excited the sample with 640 nm high-intensity illumination between frames 100 and 101. This photobleaching of the acceptor shows conversion of FRET puncta into donor emission puncta, further confirming that the signal is due to single-molecule LR probes. This conversion can be visualized by comparing frames 100 to 101 in Figure 2c. As before, a representative time trace of donor and FRET intensities is shown in Figure 2d with the probe beginning in the sheared state (frames 0–100, low donor and high FRET). Next, acceptor photobleaching occurs after frame 100, diminishing FRET signal and causing an increase in donor Cy3B emission (frames 100–155, high donor and low FRET). Finally, the Cy3B donor photobleaches, leading to single-step termination of the donor signal (frames 156 onward, low donor and low FRET). Above the intensity trajectory in Figure 2d we mark with a red line the sheared state, and we mark with a light-purple line the acceptor photobleached state. Importantly, the low donor/high FRET signal characterizing the sheared state (Figure 2d, red line) is starkly different from the high donor/low FRET signal representing the opened state (Figure 2b, green line). Lastly, all traces show single-step transitions between states and single-step termination due to photobleaching, validating that these characteristic signals are identifiable at the single-molecule level. Further controls quantified the FRET efficiency of the sheared state, yielding $FE = 85.5 \pm 7\%$ which is consistent with the donor–acceptor distance of the sheared state (Figure S5). Finally, a simulation using oxDNA was run, determining an ($F_{\text{shear}} - F_{\text{open}}$) force difference of 47.7 pN, comparable to the expected 42.3 pN for the LR probe (Figure S8, SI Note 6, OxDNA modeling of the LR Probe).

Single-Molecule LR Probe Measurements in Cell Adhesions. We next performed experiments measuring live-cell integrin forces on the LR probes. We used NIH-3T3 fibroblast cells for our live cell experiments as fibroblasts are one of the most extensively studied models for integrin mechanotransduction.³⁸ Cells were seeded onto the LR probe surface for 25 min (37C, 5% CO₂, and 5% FBS FluoroBrite DMEM) allowing cells to spread then timelapse total internal reflective fluorescence (TIRF) imaging was initiated. We alternated between reflection interference contrast microscopy (RICM) imaging and simultaneous donor/FRET imaging at a rate of 0.1 Hz over the course of the experiment spanning 100 min (Figure 3a). Figure 3b shows an overlay of the three channels at the initiation of the imaging ($t = 0$ min). Since the cells had already begun interacting with the surface, fluorescent signal from previously opened/sheared probes can be seen, with spatially distinct puncta indicating LR probe detection under single-molecule conditions (Figures 3b and S9). To study the loading rate exerted by NIH-3T3 cells, we identified single-molecule traces that followed the specific sequence of transitions described above (Figure 1f): closed state (4.7 pN) \rightarrow opened state (4.7 pN) \rightarrow sheared state (47 pN). These transitions were detected by distinct fluorescence signal outputs: a dark state (marking the closed state), an increase in Cy3B donor signal (marking the closed-to-opened state), and finally a simultaneous decrease in Cy3B donor signal and increase in FRET signal (marking the opened-to-sheared transition). A representative trace is shown in Figure 3c, with its spatial

position relative to the cell marked by an arrow in Figure 3b. Additionally, Figure 3c marks the opened, sheared, and closed states with a green, red, and gray line, respectively, above the intensity trace timestamp. These transitions and their timestamps are amenable to manual quantification; however, we created custom code to fully automate analysis and increase the throughput to handle large data sets containing tens of thousands of puncta across hundreds of frames.

Our custom Matlab codes are extensively described in SI Note 7, Automated Analysis of Single-Molecule Data. Briefly, each point of signal was fit to a 2D-Gaussian to find spatially distinct single-molecule events. Next, intensities belonging to individual LR probes were identified and clustered together, and time traces for these single-molecule events were analyzed with a changepoint algorithm to identify state transitions and their kinetics.³⁹ The evolution of the cell's interaction with the surface and the localization of real-time shearing events of LR probes are visualized in Figure 3d. Each subsequent image in Figure 3d shows an overlay of three channels (RICM, donor, FRET) at 20 min intervals and marks the location of a detected shearing event with a red circle. Shearing events are carried over between frames as black circles, so the history of high-force interactions can be visualized at later timeframes. This sequence of images has been reproduced into a video with full time resolution (SI Video 1), along with each single-molecule fluorescence trace (SI Video 2). We recommend that readers watch these videos now if able, as they help visualize the raw data while also displaying the wealth of information made available through single-molecule experiments using the LR probe. As can be seen in SI Videos 1 and 2, and Figure 3d, the vast majority of shearing events ($F > 47$ pN) occur near the periphery of the cell, a phenomenon repeatedly observed in past work.^{11,17,40} In addition to the spatial information obtained from identifying shearing events, temporal information on the cell force loading rate can be derived from the fluorescence intensity traces. Ten representative traces exhibiting a shearing event are shown in Figure 3e, with a number 1–10 indexing their spatial coordinates according to Figure 3d. Within the traces, the green arrow indicates the time of probe opening (t_{open}) and the red arrow indicates the time of probe shearing (t_{shear}), and these are automatically derived from the changepoint analysis. The color of the horizontal bar above the plot indicates the state of the probe: a green line represents the opened state, a red line represents the sheared state, and a light-purple line (when applicable) represents the acceptor photobleached state before donor photobleaching (which terminates the signal). Note that after the LR is measured (closed \rightarrow opened \rightarrow sheared), the single-molecule fluorescence signal should be terminated by single-step photobleaching, either of the donor or the acceptor. In Figure 3c, we highlight an event where the acceptor fluorophore photobleaches first, followed by the donor photobleaching (with timestamps between acceptor and donor photobleaching depicted with a horizontal purple line). This acceptor-first photobleaching occurs visibly for traces 2, 5, and 6 in Figure 3e. Other traces in Figure 3e exhibit a donor-first photobleaching, where both donor and sensitized FRET signals terminate simultaneously. Importantly, it is the duration of the opened state (length of the green line and the time difference between the green and red arrows, $t_{\text{shear}} - t_{\text{open}}$) that is used to quantify the loading time and hence the loading rate.

By repeating the analysis shown in Figure 3, we identified 138 traces from 8 NIH-3T3 cell time lapses which displayed

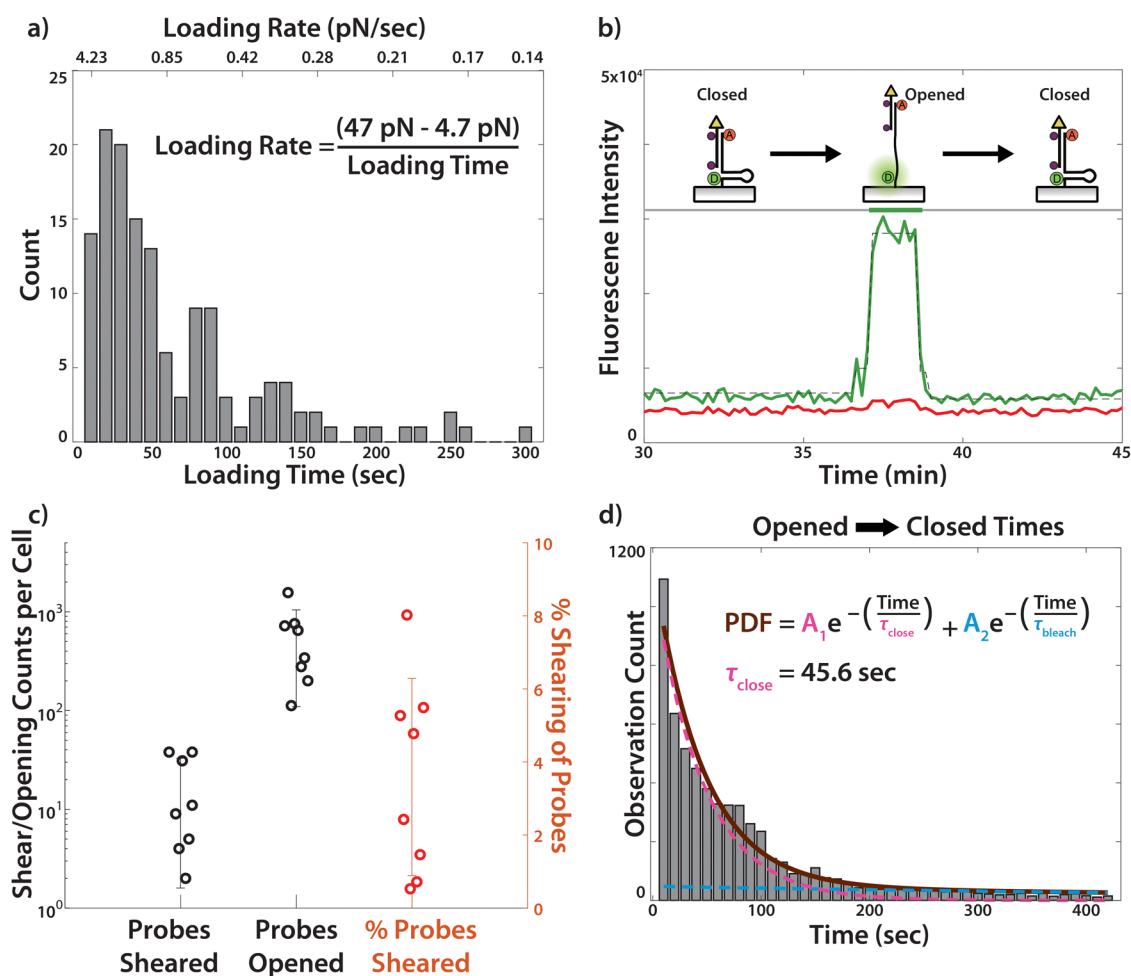


Figure 4. Analysis of LR probe live cell dynamics. (a) Histogram of loading times (bottom axis). The inset equation shows how these values are converted to a loading rate (top axis). (b) Fluorescent time trace of a closed \rightarrow opened \rightarrow closed event, with a depiction of the probe states. Donor fluorescence is in green, FRET in red, and a dotted black line marks the changepoint algorithm used to detect the transition. This trace was obtained from the dataset shown in Figure 3. (c) Plot depicting LR probe event counts from eight cells imaged for a duration of 100 min or less. The plot shows shearing and opening events for each cell as well as the ratio of opening events that leads to shearing events. (d) Histogram of times for each opened event ($N = 5981$) obtained from eight cells. The distribution was fit to a biexponential (solid brown) composed of a fixed photobleaching rate (dotted blue) and variable closing time (dotted pink), where the weights of both exponentials (A_1, A_2) were allowed to vary.

the opening \rightarrow shearing transition and quantified their loading times (Figure 4a). Observed loading times ranged from 1 to 30 frames, with mean, median, and modal loading times of 66, 40, and 20 s, respectively. In all cases, the loading rates were shorter than the average photobleaching rate of Cy3B under our conditions (71 frames, Figure S5). To derive the LR, we assume a linear loading rate between the initial hairpin opening (4.7 pN) and duplex shearing (47 pN), and divide this force difference by the observed loading time (Figure 4a, equation, and top x -axis). This calculation results in an observed median loading rate of 1.1 pN s^{-1} (with an interquartile range of $0.47\text{--}2.12 \text{ pN s}^{-1}$) exerted by live cell integrins under initial adhesion formations.

While the focus thus far has been on the closed \rightarrow opened \rightarrow sheared transitions as quantified by the LR probe, the measurements also contain information on the closed \rightarrow opened \rightarrow closed transitions (Figure 4b). These events represent forces exerted by the cell which exceed 4.7 pN, but never reach the 47 pN threshold required to shear the probe. Identifying these events (see SI Note 7.5, Identifying Closed \rightarrow Opened \rightarrow Closed Transitions) allows us to compare the number of “probes sheared” events to the number of “probes

opened” events; a proxy to the dynamics of integrin adhesion formation which are often described by binding rates (Figure 4c).^{41,42} On average, 3.6% of opened probes resulted in a shearing event, with some highly active cells shearing as many as 8.0% of opened probes (Figure 4c). In addition to the number of “probe opened” events observed, we also quantified the time during which the probe remained open before transitioning back to a closed state (as represented in Figure 4b). The time scales for these closed \rightarrow opened \rightarrow closed events are histogrammed in Figure 4d ($N = 5981$), and the probability distribution function (PDF) of all events <420 s were fit to a biexponential decay (brown line) composed of the rate of photobleaching (blue dotted line, $\tau_{\text{bleach}} = 710 \text{ s}$, Figure S5) and the rate of closing (pink dotted line, $\tau_{\text{close}} = 45.6 \pm 7.0 \text{ s}$, 95% CI), with relative amplitudes of A_1 and A_2 , respectively. A video showing the spatial location of closed \rightarrow opened \rightarrow closed transitions is included in SI Video 3, and demonstrates that most events are at the cell periphery, consistent with the regions of greatest mechanical activity.^{11,17} Examination of SI Video 3 shows very few ($<3\%$) closed \rightarrow opened \rightarrow closed transitions occurring outside the periphery of the cell. These transitions are likely due to subsequent rapid photobleaching

of the quencher/donor pair, or spontaneous opening of the LR probe (hairpin breathing). Note that spontaneous opening of the LR probe hairpin was infrequent due to the significant energy requirement for hairpin opening of $\sim 6 \times k_bT$.²⁸ Regardless, thermal hairpin opening will not affect LR measurements because of the two-step nature of the LR probe (closed \rightarrow opened \rightarrow sheared), which ignores false signals due to hairpin breathing. Finally, note that the data reported in Figure 4b–d and SI Video 3 are for these closed \rightarrow opened \rightarrow closed events, and are categorically distinct from the closed \rightarrow opened \rightarrow sheared events reported in Figure 4a and SI Videos 1–2 which are used to quantify the loading rate.

DISCUSSION

The loading rate of integrin traction forces is an important metric in describing and predicting focal adhesion dynamics.²⁴ Therefore, we anticipate that LR measurements may improve integration between experiments and molecular clutch modeling of adhesions. The LR probe reveals several features of integrin force dynamics. First, only a small subset of integrins that initially engage RGD ligands and apply low levels of force (>5 pN) proceed to ramping force to 47 pN. Over 90% of integrin–ligand complexes that experience $F > 5$ pN return to the idle state at low force. This shows that integrin–ECM mechanical sampling is highly dynamic. Our reported loading rate is derived from events that lead to shearing (closed \rightarrow opened \rightarrow sheared sequence). Thus, the reported LR represents a subset of all mechanical events: those which mature to 47 pN. Second, the lifetime of the low-magnitude mechanical force (>5 pN) decays exponentially and displays a characteristic lifetime of 45.6 s. This is consistent with integrin–ligand lifetime measurements that have ranged from 1 to hundreds of seconds.^{43,44} We note a cluster of force lifetimes between 80 and 100 s that are more frequently observed than would be anticipated from the exponential decay function in Figure 4d, and this may be due to a long-lived integrin state.⁴³ Force may terminate due to simple ligand–receptor dissociation, as the k_{off} rate of integrin–RGD bonds is well documented.⁴⁵ Alternatively, the hairpin may refold due to the termination of the force for ligated integrins. The highly dynamic mechanical nature of integrin–ligand forces reported here is consistent with reports of integrin lateral mobility and turnover within focal adhesions.^{46–48} Third, we find that force loading to 47 pN is primarily localized to the cell periphery, which spatially colocalizes with the areas that display the greatest frequency of hairpin opening events. An advantage of single-molecule force spectroscopy is the ability to correlate the loading rates for each shearing event with the spatial locations or timestamps of other shearing events. For example, one can imagine pockets of “faster” events with rapid loading rates occurring in groups around the periphery of the cell or “slower” events occurring more frequently during the initial stages of cell adhesion. We distinguished between these “fast” and “slow” events for each cell (SI Note 8, Single-cell loading rate distributions) and traced the evolution of these fast and slow assignments throughout our experiment in SI Video 11. However, we saw no obvious correlation (spatial or temporal) between loading rates of events (SI Video 11). We note that correlating the relative magnitude of LR with cellular features (e.g., focal adhesions) is difficult without a direct protein marker of adhesions, which is achievable through utilizing an additional, distinct fluorescence channel. This additional dimensionality would add significant complexity to this

experiment and is a future direction for our work. Fourth, our observed force LR is highly heterogeneous with a distribution of about a median of 1.1 pN s^{-1} . This LR is consistent with reports by Sheetz and Roca-Cusachs that estimated a loading rate of 2.5 pN s^{-1} by inference of actin retrograde flow measurements in conjunction with measurements of the force required to unfold talin.³ The same group also used loading rates obtained from traction force microscopy to infer individual integrin loading rates of 0.007 to 4 pN s^{-1} .²⁷ Note that this estimate is derived from time-dependent stress measurements and requires an assumption of the density of integrins, which can range from tens to hundreds per square micron. Lastly, during the revision of this manuscript, Jo et al.⁴⁹ and Hu et al.⁵⁰ published complementary approaches to measuring integrin loading rates and found values of $0.5\text{--}4 \text{ pN s}^{-1}$, in agreement with our work. The design by Jo et al. utilized a peeling mechanism due to overstretching of an anchor probe, as originally described by Ma et al.⁵¹ While the peeling mechanism is insensitive to forces below 20 pN due to thermal dissociation, it has the potential advantage of avoiding the issue of terminating mechanotransduction, which is well documented for shearing probes. Thus, the overstretch peeling probe offers a complementary sensor to investigate loading rates in living cells.

Past work with single-molecule force spectroscopy, such as optical tweezers and atomic force microscopy (AFM), applied force to integrin–ligand bonds and recorded the bond duration leading up to rupture. These values provide insights into bond lifetime under force, rather than the actual force lifetime or the native LR of integrin–ligand complexes within adhesions. Importantly, our LR probe measures forces generated by the cell itself and transmitted to single integrins, and the observed LR are orders of magnitude lower in magnitude compared to those induced through AFM and optical/magnetic bead techniques.^{27,52,53} Given that the ligand–receptor rupture force is highly dependent on LR, our work suggests that future single-molecule force spectroscopy experiments should tune LR to $\sim 1 \text{ pN s}^{-1}$ to better approximate physiological values.

Challenges inherent to single-molecule measurements warrant discussion. First, to accommodate the long time scale of the experiment (>1 h), the frame rate was set to 0.1 Hz, or 1 image per 10 s. Any events undergoing their transition sequence (e.g., closed \rightarrow opened \rightarrow sheared) faster than our frame rate would remain unobserved. From Figure 4a, it is clear that the bulk of the loading time distribution is successfully measured, but care must be taken when selecting an acquisition rate, which should be optimized for a given system. Second, a large number of single-molecule events (fluorescent puncta) are observed that do not follow the described sequence transition (closed \rightarrow opened \rightarrow sheared). Many photophysical or biological events can alter the fluorescent output at the single-molecule level, such as photobleaching, dye blinking, probe degradation, and heterogeneous microenvironments, including the nuclease-rich environment under the cell. Here, we set our analysis for high specificity exclusively investigating closed \rightarrow opened \rightarrow sheared events and ignoring events that fail to satisfy this sequence, some of which may be true shearing events. The strict analysis criteria are described in SI Note 7 (which screens for the closed \rightarrow opened \rightarrow sheared sequence) and results in greater fidelity as noted in SI Videos 1 and 4–10, where $>99\%$ of events occur within the periphery of the cell in contrast to nonspecific events which may occur outside the cell. Lastly, we

note one possible false shearing signal in the scenario of Q_1 bleaching, while Q_2 , donor and acceptor remaining active. This would appear as a long-lived opening event that could progress to shearing, and suggest a low LR. Such a sequence of events is not observed and highly unlikely based on our control.

CONCLUSIONS

In summary, we have developed a novel method for detecting two distinct transitions of a single molecular complex composed of two DNA strands by fluorescence dequenching followed by FRET. This probe can detect both low (>4.7 pN) and high (>47 pN) force thresholds in integrin-ECM bonds at the single-molecule level. We derive LRs for the live cell integrin mechanoreceptors which are congruent with estimates modeled in the field. This probe design protects both fluorophores from photobleaching and enables high-fidelity detection of sequential mechanical transitions of DNA strands in single molecular complexes. The LR probe can be adapted to detect different thresholds by engineering the nucleic acid geometry or DNA sequence and such tuning is needed to investigate different classes of mechanoreceptor. Finally, we note that the LR probe is not specific to integrins and the ligand can be replaced with a wide variety of peptides or proteins appropriate for the biological system of interest that may include immune receptors and other class of mechanoreceptors.^{32,54–56}

ASSOCIATED CONTENT

Supporting Information

The Supporting Information is available free of charge at <https://pubs.acs.org/doi/10.1021/jacs.4c03629>.

Detailed experimental and analytical procedures; microscopy setup diagram; modeling descriptions; synthesis procedure and characterization; probe characterization; and single-molecule validation (PDF)

Localizations of shearing events marked with red circles overlaid with an RICM image of cell #1 (Video 1) (AVI)

The same RICM timelapse as in Video 1 (Video 2) (AVI)

RICM timelapse of cell #1 (Video 3) (AVI)

Localizations of shearing events marked with red circles overlaid with an RICM image of cell #2 (Video 4) (AVI)

Localizations of shearing events marked with red circles overlaid with an RICM image of cell #3 (Video 5) (AVI)

Localizations of shearing events marked with red circles overlaid with an RICM image of cell #4 (Video 6) (AVI)

Localizations of shearing events marked with red circles overlaid with an RICM image of cell #5 (Video 7) (AVI)

Localizations of shearing events marked with red circles overlaid with an RICM image of cell #6 (Video 8) (AVI)

Localizations of shearing events marked with red circles overlaid with an RICM image of cell #7 (Video 9) (AVI)

Localizations of shearing events marked with red circles overlaid with an RICM image of cell #10 (Video 10) (AVI)

Evolution of fast and slow LR events for cell #1, marked in purple and black circles, respectively (Video 11) (AVI)

AUTHOR INFORMATION

Corresponding Author

Khalid Salaita – Department of Chemistry, Emory University, Atlanta, Georgia 30322, United States; Wallace H. Coulter Department of Biomedical Engineering, Georgia Institute of Technology and Emory University, Atlanta, Georgia 30322, United States; orcid.org/0000-0003-4138-3477; Email: k.salaita@emory.edu

Authors

J. Dale Combs – Department of Chemistry, Emory University, Atlanta, Georgia 30322, United States

Alexander K. Foote – Department of Chemistry, Emory University, Atlanta, Georgia 30322, United States

Hiroaki Ogasawara – Department of Chemistry, Emory University, Atlanta, Georgia 30322, United States; orcid.org/0000-0001-8462-562X

Arventh Velusamy – Department of Chemistry, Emory University, Atlanta, Georgia 30322, United States

Sk Aysha Rashid – Department of Chemistry, Emory University, Atlanta, Georgia 30322, United States

Joseph Nicholas Mancuso – Department of Chemistry, Emory University, Atlanta, Georgia 30322, United States

Complete contact information is available at: <https://pubs.acs.org/doi/10.1021/jacs.4c03629>

Author Contributions

§J.D.C. and A.K.F. contributed equally to this work. The manuscript was written through contributions of all authors. All authors have given approval to the final version of the manuscript.

Notes

The authors declare no competing financial interest.

ACKNOWLEDGMENTS

K.S. acknowledges support from NIH NIAID R01AI172452 and NIGMS R01GM131099 and 1RM1GM145394.

REFERENCES

- (1) Martino, F.; Perestrelo, A. R.; Vinarský, V.; Pagliari, S.; Forte, G. Cellular Mechanotransduction: From Tension to Function. *Front. Physiol.* **2018**, *9*, No. 824.
- (2) Jaalouk, D. E.; Lammerding, J. Mechanotransduction Gone Awry. *Nat. Rev. Mol. Cell Biol.* **2009**, *10* (1), 63–73.
- (3) Roca-Cusachs, P.; Iskratsch, T.; Sheetz, M. P. Finding the Weakest Link-Exploring Integrin-Mediated Mechanical Molecular Pathways. *J. Cell Sci.* **2012**, *125* (13), 3025–3038.
- (4) Uroz, M.; Wistorf, S.; Serra-Picamal, X.; Conte, V.; Sales-Pardo, M.; Roca-Cusachs, P.; Guimerà, R.; Trepac, X. Regulation of Cell Cycle Progression by Cell-Cell and Cell-Matrix Forces. *Nat. Cell Biol.* **2018**, *20* (6), 646–654.
- (5) Henderson, N. C.; Arnold, T. D.; Katamura, Y.; Giacomini, M. M.; Rodriguez, J. D.; McCarty, J. H.; Pellicoro, A.; Raschperger, E.; Betsholtz, C.; Ruminski, P. G.; Griggs, D. W.; Prinsen, M. J.; Maher, J. J.; Iredale, J. P.; Lacy-Hulbert, A.; Adams, R. H.; Sheppard, D. Targeting of α Integrin Identifies a Core Molecular Pathway That Regulates Fibrosis in Several Organs. *Nat. Med.* **2013**, *19* (12), 1617–1624.
- (6) Mierke, C. T.; Frey, B.; Fellner, M.; Herrmann, M.; Fabry, B. Integrin $A5\beta 1$ Facilitates Cancer Cell Invasion through Enhanced Contractile Forces. *J. Cell Sci.* **2011**, *124* (3), 369–383.
- (7) Abenza, J. F.; Rossetti, L.; Mouelhi, M.; Burgués, J.; Andreu, I.; Kennedy, K.; Roca-Cusachs, P.; Marco, S.; García-Ojalvo, J.; Trepac,

- X. Mechanical Control of the Mammalian Circadian Clock via YAP/TAZ and TEAD. *J. Cell Biol.* **2023**, *222* (9), No. e202209120.
- (8) Oriá, R.; Wiegand, T.; Escribano, J.; Elosegui-Artola, A.; Uriarte, J. J.; Moreno-Pulido, C.; Platzman, I.; Delcanale, P.; Albertazzi, L.; Navajas, D.; Trepát, X.; García-Aznar, J. M.; Cavalcanti-Adam, E. A.; Roca-Cusachs, P. Force Loading Explains Spatial Sensing of Ligands by Cells. *Nature* **2017**, *552* (7684), 219–224.
- (9) Stabley, D. R.; Jurchenko, C.; Marshall, S. S.; Salaita, K. S. Visualizing Mechanical Tension across Membrane Receptors with a Fluorescent Sensor. *Nat. Methods* **2012**, *9* (1), 64–67.
- (10) Liu, Y.; Yehl, K.; Narui, Y.; Salaita, K. Tension Sensing Nanoparticles for Mechano-Imaging at the Living/Nonliving Interface. *J. Am. Chem. Soc.* **2013**, *135* (14), 5320–5323.
- (11) Zhang, Y.; Ge, C.; Zhu, C.; Salaita, K. DNA-Based Digital Tension Probes Reveal Integrin Forces during Early Cell Adhesion. *Nat. Commun.* **2014**, *5*, No. 5167.
- (12) Galior, K.; Liu, Y.; Yehl, K.; Vivek, S.; Salaita, K. Titin-Based Nanoparticle Tension Sensors Map High-Magnitude Integrin Forces within Focal Adhesions. *Nano Lett.* **2016**, *16* (1), 341–348.
- (13) Jurchenko, C.; Salaita, K. S. Lighting Up the Force: Investigating Mechanisms of Mechanotransduction Using Fluorescent Tension Probes. *Mol. Cell Biol.* **2015**, *35* (15), 2570–2582.
- (14) Liu, Y.; Galior, K.; Ma, V. P. Y.; Salaita, K. Molecular Tension Probes for Imaging Forces at the Cell Surface. *Acc. Chem. Res.* **2017**, *50* (12), 2915–2924.
- (15) Ma, V. P. Y.; Salaita, K. DNA Nanotechnology as an Emerging Tool to Study Mechanotransduction in Living Systems. *Small* **2019**, *15* (26), No. 1900961.
- (16) Hu, Y.; Duan, Y.; Salaita, K. DNA Nanotechnology for Investigating Mechanical Signaling in the Immune System. *Angew. Chem., Int. Ed.* **2023**, *62* (30), No. e202302967.
- (17) Wang, Y.; Wang, X. Integrins Outside Focal Adhesions Transmit Tensions during Stable Cell Adhesion. *Sci. Rep.* **2016**, *6*, No. 36959.
- (18) Rashid, S. A.; Blanchard, A. T.; Combs, J. D.; Fernandez, N.; Dong, Y.; Cho, H. C.; Salaita, K. DNA Tension Probes Show That Cardiomyocyte Maturation Is Sensitive to the Piconewton Traction Forces Transmitted by Integrins. *ACS Nano* **2022**, *16* (4), 5335–5348.
- (19) Jo, M. H.; Li, J.; Jaumouillé, V.; Hao, Y.; Coppola, J.; Yan, J.; Waterman, C. M.; Springer, T. A.; Ha, T. Single-Molecule Characterization of Subtype-Specific B1 Integrin Mechanics. *Nat. Commun.* **2022**, *13* (1), No. 7471.
- (20) Zhang, Y.; Qiu, Y.; Blanchard, A. T.; Chang, Y.; Brockman, J. M.; Ma, V. P. Y.; Lam, W. A.; Salaita, K. Platelet Integrins Exhibit Anisotropic Mechanosensing and Harness Piconewton Forces to Mediate Platelet Aggregation. *Proc. Natl. Acad. Sci. U.S.A.* **2018**, *115* (2), 325–330.
- (21) Ma, V. P.-Y.; Hu, Y.; Kellner, A. V.; Brockman, J. M.; Velusamy, A.; Blanchard, A. T.; Evavold, B. D.; Alon, R.; Salaita, K. The Magnitude of LFA-1/ICAM-1 Forces Fine-Tune TCR-Triggered T Cell Activation. *Sci. Adv.* **2022**, *8* (8), No. eabg4485.
- (22) Andreu, I.; Falcones, B.; Hurst, S.; Chahare, N.; Quiroga, X.; Le Roux, A. L.; Kechagia, Z.; Beedle, A. E. M.; Elosegui-Artola, A.; Trepát, X.; Farré, R.; Betz, T.; Almendros, I.; Roca-Cusachs, P. The Force Loading Rate Drives Cell Mechanosensing through Both Reinforcement and Cytoskeletal Softening. *Nat. Commun.* **2021**, *12* (1), No. 4229.
- (23) Chan, C. E.; Odde, D. J. Traction Dynamics of Filopodia on Compliant Substrates. *Science* **2008**, *322* (5908), 1687–1691.
- (24) Elosegui-Artola, A.; Trepát, X.; Roca-Cusachs, P. Control of Mechanotransduction by Molecular Clutch Dynamics. *Trends Cell Biol.* **2018**, *28* (5), 356–367.
- (25) Ley, K.; Rivera-Nieves, J.; Sandborn, W. J.; Shattil, S. Integrin-Based Therapeutics: Biological Basis, Clinical Use and New Drugs. *Nat. Rev. Drug Discovery* **2016**, *15* (3), 173–183.
- (26) Slack, R. J.; Macdonald, S. J. F.; Roper, J. A.; Jenkins, R. G.; Hatley, R. J. D. Emerging Therapeutic Opportunities for Integrin Inhibitors. *Nat. Rev. Drug Discovery* **2022**, *21* (1), 60–78.
- (27) Moore, S. W.; Roca-Cusachs, P.; Sheetz, M. P. Stretchy Proteins on Stretchy Substrates: The Important Elements of Integrin-Mediated Rigidity Sensing. *Dev. Cell* **2010**, *19* (2), 194–206.
- (28) Woodside, M. T.; Behnke-Parks, W. M.; Larizadeh, K.; Travers, K.; Herschlag, D.; Block, S. M. Nanomechanical Measurements of the Sequence-Dependent Folding Landscapes of Single Nucleic Acid Hairpins. *Proc. Natl. Acad. Sci. U.S.A.* **2006**, *103* (16), 6190–6195.
- (29) Chang, A. C.; Mekhdjian, A. H.; Morimatsu, M.; Denisin, A. K.; Pruitt, B. L.; Dunn, A. R. Single Molecule Force Measurements in Living Cells Reveal a Minimally Tensioned Integrin State. *ACS Nano* **2016**, *10* (12), 10745–10752.
- (30) Tan, S. J.; Chang, A. C.; Anderson, S. M.; Miller, C. M.; Prahll, L. S.; Odde, D. J.; Dunn, A. R. Regulation and Dynamics of Force Transmission at Individual Cell-Matrix Adhesion Bonds. *Sci. Adv.* **2020**, *6* (20), No. eaax0317.
- (31) Göhring, J.; Kellner, F.; Schrangl, L.; Platzler, R.; Klotzsch, E.; Stockinger, H.; Huppa, J. B.; Schütz, G. J. Temporal Analysis of T-Cell Receptor-Imposed Forces via Quantitative Single Molecule FRET Measurements. *Nat. Commun.* **2021**, *12* (1), No. 2502.
- (32) Wang, X.; Ha, T. Single Molecular Forces Required to Activate Integrin and Notch Signaling. *Science* **2013**, *340* (6135), 991–994.
- (33) Hatch, K.; Danilowicz, C.; Coljee, V.; Prentiss, M. Demonstration That the Shear Force Required to Separate Short Double-Stranded DNA Does Not Increase Significantly with Sequence Length for Sequences Longer than 25 Base Pairs. *Phys. Rev. E: Stat., Nonlinear, Soft Matter Phys.* **2008**, *78* (1), No. 011920.
- (34) Liu, J.; Yan, J. Unraveling the Dual-Stretch-Mode Impact on Tension Gauge Tethers' Mechanical Stability. *J. Am. Chem. Soc.* **2024**, *146* (11), 7266–7273.
- (35) Gidi, Y.; Bayram, S.; Ablenas, C. J.; Blum, A. S.; Cosa, G. Efficient One-Step PEG-Silane Passivation of Glass Surfaces for Single-Molecule Fluorescence Studies. *ACS Appl. Mater. Interfaces* **2018**, *10* (46), 39505–39511.
- (36) Glazier, R.; Shinde, P.; Ogasawara, H.; Salaita, K. Spectroscopic Analysis of a Library of DNA Tension Probes for Mapping Cellular Forces at Fluid Interfaces. *ACS Appl. Mater. Interfaces* **2021**, *13* (2), 2145–2164.
- (37) Ma, R.; Kellner, A. V.; Ma, V. P.-Y.; Su, H.; Deal, B. R.; Brockman, J. M.; Salaita, K. DNA Probes That Store Mechanical Information Reveal Transient Piconewton Forces Applied by T Cells. *Proc. Natl. Acad. Sci. U.S.A.* **2019**, *116* (34), 16949–16954.
- (38) D'Urso, M.; Kurniawan, N. A. Mechanical and Physical Regulation of Fibroblast–Myofibroblast Transition: From Cellular Mechanoreponse to Tissue Pathology. *Front. Bioeng. Biotechnol.* **2020**, *8*, No. 609653.
- (39) Killick, R.; Fearnhead, P.; Eckley, I. A. Optimal Detection of Changepoints with a Linear Computational Cost. *J. Am. Stat. Assoc.* **2012**, *107*, 1590–1598.
- (40) Rashid, S. A.; Dong, Y.; Ogasawara, H.; Vierengel, M.; Essien, M. E.; Salaita, K. All-Covalent Nuclease-Resistant and Hydrogel-Tethered DNA Hairpin Probes Map PN Cell Traction Forces. *ACS Appl. Mater. Interfaces* **2023**, *15* (28), 33362–33372.
- (41) Tsunoyama, T. A.; Watanabe, Y.; Goto, J.; Naito, K.; Kasai, R. S.; Suzuki, K. G. N.; Fujiwara, T. K.; Kusumi, A. Super-Long Single-Molecule Tracking Reveals Dynamic-Anchorage-Induced Integrin Function. *Nat. Chem. Biol.* **2018**, *14* (5), 497–506.
- (42) Fischer, L. S.; Klingner, C.; Schlichthaerle, T.; Strauss, M. T.; Bötcher, R.; Fässler, R.; Jungmann, R.; Grashoff, C. Quantitative Single-Protein Imaging Reveals Molecular Complex Formation of Integrin, Talin, and Kindlin during Cell Adhesion. *Nat. Commun.* **2021**, *12* (1), No. 919.
- (43) Kong, F.; Li, Z.; Parks, W. M.; Dumbauld, D. W.; García, A. J.; Mould, A. P.; Humphries, M. J.; Zhu, C. Cyclic Mechanical Reinforcement of Integrin-Ligand Interactions. *Mol. Cell* **2013**, *49* (6), 1060–1068.
- (44) Kong, F.; García, A. J.; Mould, A. P.; Humphries, M. J.; Zhu, C. Demonstration of Catch Bonds between an Integrin and Its Ligand. *J. Cell Biol.* **2009**, *185* (7), 1275–1284.

(45) Kapp, T. G.; Rechenmacher, F.; Neubauer, S.; Maltsev, O. V.; Cavalcanti-Adam, E. A.; Zarka, R.; Reuning, U.; Notni, J.; Wester, H. J.; Mas-Moruno, C.; Spatz, J.; Geiger, B.; Kessler, H. A Comprehensive Evaluation of the Activity and Selectivity Profile of Ligands for RGD-Binding Integrins. *Sci. Rep.* **2017**, *7*, No. 39805.

(46) Margadant, C.; Kreft, M.; Zambruno, G.; Sonnenberg, A. Kindlin-1 Regulates Integrin Dynamics and Adhesion Turnover. *PLoS One* **2013**, *8* (6), No. e65341.

(47) López-Ceballos, P.; Herrera-Reyes, A. D.; Coombs, D.; Tanentzapf, G. In Vivo Regulation of Integrin Turnover by Outside-in Activation. *J. Cell Sci.* **2016**, *129* (15), 2912–2924.

(48) Bakker, G. J.; Eich, C.; Torreno-Pina, J. A.; Diez-Ahedo, R.; Perez-Samper, G.; Van Zanten, T. S.; Figdor, C. G.; Cambi, A.; Garcia-Parajo, M. F. Lateral Mobility of Individual Integrin Nanoclusters Orchestrates the Onset for Leukocyte Adhesion. *Proc. Natl. Acad. Sci. U.S.A.* **2012**, *109* (13), 4869–4874.

(49) Jo, M. H.; Meneses, P.; Yang, O.; Carcamo, C. C.; Pangeni, S.; Ha, T. Determination of Single-Molecule Loading Rate during Mechanotransduction in Cell Adhesion. *Science* **2024**, *383* (6689), 1374–1379.

(50) Hu, Y.; Li, H.; Zhang, C.; Feng, J.; Wang, W.; Chen, W.; Yu, M.; Liu, X.; Zhang, X.; Liu, Z. DNA-based ForceChrono probes for deciphering single-molecule force dynamics in living cells. *Cell* **2024**, *187*, 3445–3459.

(51) Ma, R.; Rashid, S. A.; Velusamy, A.; Deal, B. R.; Chen, W.; Petrich, B.; Li, R.; Salaita, K. Molecular Mechanocytometry Using Tension-Activated Cell Tagging. *Nat. Methods* **2023**, *20* (11), 1666–1671.

(52) Li, F.; Redick, S. D.; Erickson, H. P.; Moy, V. T. Force Measurements of the $\text{A5}\beta\text{1}$ Integrin–Fibronectin Interaction. *Biophys. J.* **2003**, *84* (2), 1252–1262.

(53) Burgos-Bravo, F.; Martínez-Meza, S.; Quest, A. F. G.; Wilson, C. A. M.; Leyton, L. Application of Force to a Syndecan-4 Containing Complex With Thy-1– $\text{AV}\beta\text{3}$ Integrin Accelerates Neurite Retraction. *Front. Mol. Biosci.* **2020**, *7*, No. 582257.

(54) Liu, Y.; Blanchfield, L.; Ma, V. P.-Y.; Andargachew, R.; Gailor, K.; Zheng, L.; Evavold, B.; Salaita, K. DNA-based nanoparticle tension sensors reveal that T-cell receptors transmit defined pN forces to their antigens for enhanced fidelity. *Proc. Natl. Acad. Sci. U.S.A.* **2016**, *113* (20), 5610–5615.

(55) Wan, Z.; Xu, C.; Chen, X.; Xie, H.; Li, Z.; Wang, J.; Ji, X.; Chen, H.; Ji, Q.; Shaheen, S.; Xu, Y.; Wang, F.; Tang, J.-S.; Zheng, J. S.; Chen, W.; Lou, J.; Liu, W. $\text{PI}(4,5)\text{P}_2$ determines the threshold of mechanical force-induced B cell activation. *J. Cell Biol.* **2018**, *217* (7), 2565–2582.

(56) Zhao, B.; Li, B.; Xie, T.; Bagheri, Y.; Liang, C.; Keshri, P.; Sun, Y.; You, M. Quantifying tensile forces at cell–cell junctions with a DNA-based fluorescent probe. *Chem. Sci.* **2020**, *11*, 8558–8566.